buildings

MDPI

Article

Research on Mechanical Characteristics of High-Toughness Anti-Slip Pile Based on Slope Anti-Slip Stability Enhancement

Changzhu Xing [1], Yanwei Yang [1], Chuanfeng Zheng [2,*], Dayu Liu [1], Haigang Li [1], Liying Guo [1], Weitao Lin [1] and Chengda Wang [1]

[1] Originwater Construction Group Co., Ltd., Beijing 100000, China; changzhuxing@163.com (C.X.)
[2] College of Transportation, Jilin University, Changchun 130012, China
* Correspondence: cfzheng@jlu.edu.cn

Abstract: Aiming at the problem of insufficient slope stability in deep foundation pit engineering, this paper takes the integrated urban and rural water supply project in Lingao County as the research object, simulates and analyzes the landslide process of the slope by using the strength discount method, and explores the mechanical response characteristics of the anti-slip piles in depth. It is found that the traditional anti-slip pile is prone to early failure due to bending and tensile damage in the middle of the pile back, which leads to the decline of slope stability. For this reason, this paper designs and studies the high-toughness anti-slip pile material and carries out numerical simulation analyses on C30 concrete anti-slip piles and high-toughness concrete anti-slip piles, respectively, for 9 working conditions, for a total of 18 working conditions. The results show that the bending and tensile toughness and strength of the anti-slip piles are significantly improved by using high-toughness material, which effectively avoids bending and tensile damage, and the slope safety coefficient is increased by 32.10%. Furthermore, the optimized design of anti-slip piles in terms of material, pile length, and pile position can effectively improve the stability of slopes and prolong the service life of the anti-slip piles, which provides a new way of thinking and methodology for the safety design of the deep foundation pit project. Thus, this study has important theoretical significance and engineering application value.

Keywords: deep foundation pits; graded slopes; high-tenacity anti-slip piles; mechanical response

Citation: Xing, C.; Yang, Y.; Zheng, C.; Liu, D.; Li, H.; Guo, L.; Lin, W.; Wang, C. Research on Mechanical Characteristics of High-Toughness Anti-Slip Pile Based on Slope Anti-Slip Stability Enhancement. *Buildings* **2024**, *14*, 3641. https://doi.org/10.3390/buildings14113641

Academic Editor: Harry Far

Received: 16 October 2024
Revised: 8 November 2024
Accepted: 12 November 2024
Published: 15 November 2024

1. Introduction

China's complex and diverse landscape poses significant challenges in engineering fields such as foundation pit excavation and railway construction in gorges, where slope stability is a critical concern. As infrastructure development accelerates, the number of deep foundation pit projects increases, heightening the safety risks posed by landslides during slope excavation. Without effective protective measures, sliding soil masses can destabilize foundation pits, leading to soil burial accidents, causing substantial project losses, and threatening the safety of construction workers [1,2]. Therefore, how to effectively improve slope stability has become an urgent problem we aim to address in this project.

Anti-slide piles are commonly used reinforcement measures in engineering due to their simple structure, ease of construction, and significant effectiveness in enhancing slope safety [3,4]. Typically, anti-slide piles penetrate the sliding surface of the slope and are embedded into stable layers to enhance slope stability. These piles mainly resist the lateral thrust of sliding soil masses while relying on the soil in front of the piles for additional resistance [5,6]. Various factors can lead to the failure of anti-slide piles, including pile breakage or shear failure, pile overturning, soil mass flowing between piles, and soil surging over the pile tops [7–9]. In recent years, researchers have made notable progress in understanding the failure mechanisms of anti-slide piles, particularly in pile stress analysis and the distribution of landslide thrust. Numerical simulations and model tests

were employed to optimize the mechanical performance of anti-slide piles, focusing on improving their bending and shear strength to mitigate the destructive effects of lateral landslide thrust on the piles [10].

To deeply study the role of anti-slip piles in slope reinforcement, this paper relies on the integrated urban and rural water supply project in Lingao County, uses the strength discount method to simulate the slope landslide disaster, and explores the change rule of the slope safety coefficient under the action of ordinary concrete anti-slip piles and high-toughness anti-slip piles, respectively. This study also conducts an in-depth analysis of the mechanical response of the anti-slip piles in the process of force and arrives at the impact of anti-slip piles on the slope stability. This paper concludes that the key influencing factors and the superiority of high-toughness material anti-slip piles in the process of slope stabilization have an important reference value for improving the effect of slope reinforcement and optimizing the safety design of deep foundation pit projects.

2. Project Overview

This study is based on the Urban-Rural Integration Water Supply Project in Lingao County, where a southern water treatment plant is planned for construction. The existing ground elevation of the intake pump station site ranges from 104 to 110.5 m. The excavation will follow a staged slope to the current ground level, with the design elevation of the pump station pit bottom set at 91.95 m. The excavation depth will range from approximately 12.05 to 18.55 m. The existing ground elevation of the intake pipeline site is between 94 and 106 m, and it will also follow a staged slope to the current ground level. The design elevation of the pipeline pit bottom is 94.65 m, with an excavation depth ranging from 0 to 11.35 m. The excavation for both the pump station and the intake pipeline will be combined, covering an area of approximately 8819.86 m^2 at the top edge.

The existing ground elevation within the plant area varies from 104.0 to 111.3 m, and the leveling elevation is set between 106 and 110.5 m. The design elevation of the pit bottoms for the various structures ranges from 102.5 to 109.5 m. Except for independently excavated structures, all other foundation pits in the plant area are combined into one large excavation. The excavation depth for the combined foundation pit ranges from 1.0 to 7.2 m.

To analyze the stability of the slope soil, this study employs the ABAQUS finite element software (version number: 2020HF5) to perform numerical simulations on a typical slope case [11]. The dimensional information of slopes and material properties of soil layers can be obtained from design documents of the dependent projects. The dimensions of the slope soil model and the location of the anti-slip pile assembly are shown in Figure 1. The slope height is 10 m with a slope ratio of 1:1.5. The distance from the slope to the front and rear boundaries is 2.5 times the slope height (i.e., 25 m), and the distance from the slope to the bottom boundary is three times the slope height (i.e., 30 m). The stretching thickness of the soil in the z-direction is 4 m. The material parameters of the slope soil are listed in Table 1. Normal constraints are applied to all four sides of the slope, while the bottom is set with a fixed constraint. In the numerical simulation of unsupported slopes, the approximate global size of the grid is 0.8 m, the cell type is C3D8R, and the meshing method is swept; in the numerical simulation of supported slopes, the approximate global size of the grid is 1 m, the cell type is C3D8R, and the meshing method is structural. The contact between the skid pile and the soil is normal hard contact with tangential friction contact with a coefficient of friction of 0.3 [12].

Table 1. Material parameters of the slope soil.

Density (kN/m^3)	Poisson's Ratio	Elastic Modulus (MPa)	Cohesion (kPa)	Internal Friction Angle (°)
20	0.25	200	10	20

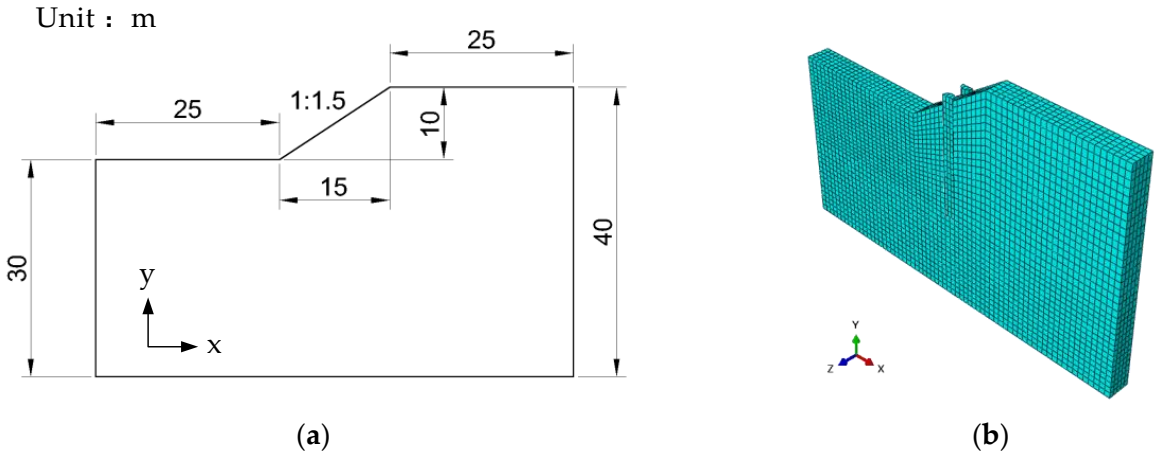

Figure 1. (**a**) Schematic diagram of the slope model; (**b**) anti-slip pile assembly diagram.

The entire calculation process is divided into two steps. The first step is the geostatic analysis, where the initial stress under gravitational force is obtained. The second step involves reducing the shear strength of the slope soil. This step is achieved by setting a field variable (FV1) and editing the model's keywords to reduce the slope soil's cohesion and internal friction angle. The field variable FV1 represents the safety factor of the slope, which varies from 0.5 to 2.0. The shear strength parameters of the soil are calculated and input into the model using the reduction formula.

The soil layer parameters are shown in Table 1.

3. Comparative Analysis of Stability Between Ordinary Materials and High-Toughness Materials in Anti-Slide Piles

3.1. Method of Analyzing Anti-Slide Stability

A numerical simulation and analysis were conducted based on a typical slope case study [13], utilizing the strength reduction method (SSRM). The Griffith method can yield a slope safety factor similar to traditional calculation methods. Compared to earlier approaches, the strength reduction method directly computes the sliding surface and safety factor of the slope, simplifying the otherwise complex process, and provides clear and intuitive results. This method has been widely accepted in engineering practice. The strength reduction method calculates the slope safety factor by determining the degree of strength reduction at the point when the slope soil reaches the critical state of failure. Specifically, the cohesion and internal friction angle of the slope soil is continuously reduced under unchanged external conditions until the slope fails. The reduction factor at this state is the slope's safety factor [14]. The formula for calculating the reduced shear strength parameters of the slope soil is as follows:

$$c_m = c/F_r, \tag{1}$$

$$\varphi_m = \arctan(\tan\varphi/F_r) \tag{2}$$

where c and ϕ represent the original shear strength parameters of the soil; cm and ϕ_m represent the reduced shear strength parameters; and Fr is the strength reduction factor.

In existing studies, there are three criteria for determining slope instability using the strength reduction method [15]: the numerical simulation fails to converge; a continuous plastic zone forms through the slope; and a sudden increase in displacement occurs at a specific point on the slope surface. Each of these methods has its advantages and disadvantages: convergence in numerical simulations depends on various factors such as the calculation method and mesh division; the formation of a continuous plastic zone is difficult to evaluate objectively; and the selection of a characteristic point can influence the sudden displacement criterion. Some researchers compared results derived from these three

criteria in practical cases and found them to be highly reliable and accurate [16]. Therefore, this study combines the three criteria for a comprehensive analysis when determining the slope safety factor, ensuring an accurate evaluation of slope instability.

3.2. Stability Analysis of Unreinforced Slopes

Three characteristic points on the slope were selected to determine the onset of rapid displacement increase, as shown in Figure 2: the slope toe (point A), the mid-slope (point B), and the slope crest (point C). The slope safety factor at the time of instability was confirmed through the FV1-U1 curve, as depicted in Figure 3. The slope crest (C) and mid-slope (B) entered instability at a safety factor of FV1 = 1.172, while the slope toe (A) became unstable at FV1 = 1.181. Therefore, FV1 = 1.172 was selected as the critical safety factor corresponding to the onset of rapid displacement. This observation suggests that the slope crest and mid-slope are more prone to failure when instability occurs. When the numerical model failed to converge, the safety factor was FV1 = 1.201 (Figure 4). When the plastic zone formed a continuous connection through the slope (Figure 5), the safety factor was FV1 = 1.172, consistent with the value at which rapid displacement occurred. Therefore, the critical safety factor for slope failure in this typical model is FV1 = 1.172. Among the three evaluation methods, the safety factor obtained using the non-convergence criterion was higher, but it may not accurately reflect the actual instability conditions. Hence, relying solely on this method could be dangerous, and a combination of the other two methods should be used to assess slope instability accurately.

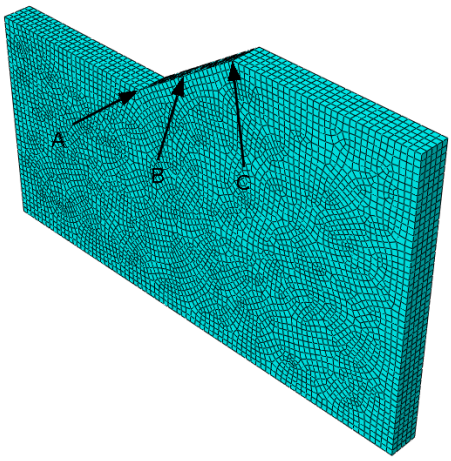

Figure 2. Model mesh division.

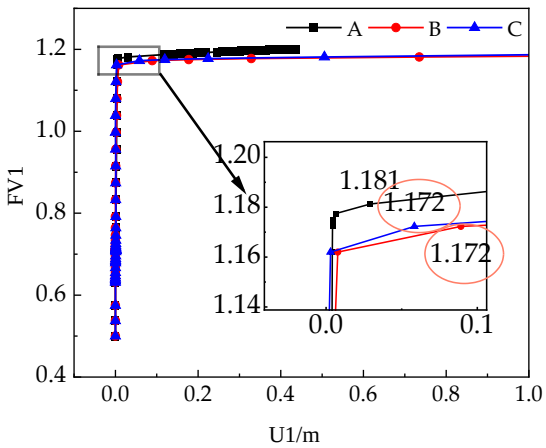

Figure 3. Safety factor–horizontal displacement at three key points on the slope.

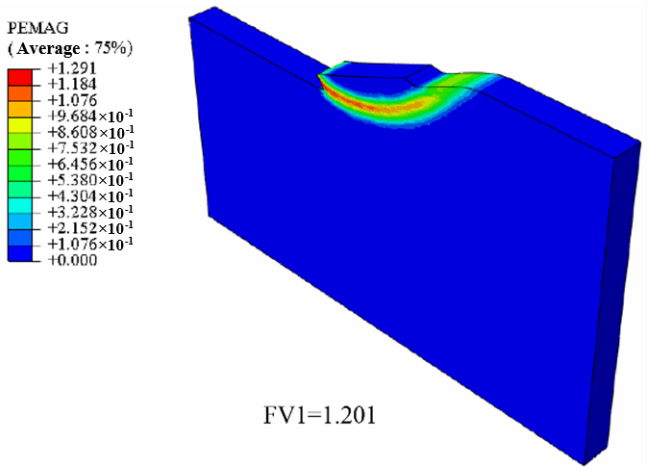

Figure 4. Safety factor–horizontal displacement at three key points on the slope.

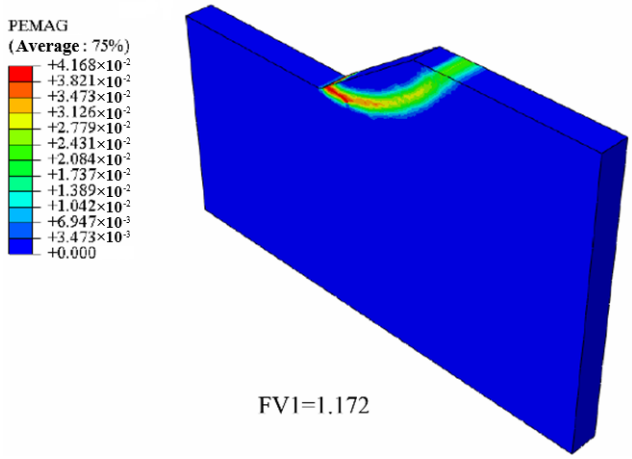

Figure 5. Equivalent plastic strain contour when the plastic zone connects.

From Figures 6 and 7, it can be seen that, when slope instability occurs, the type of landslide is a translational slide. After the upper soil becomes unstable, it slides downward along the slope, acting on the middle and lower parts of the soil, causing a progressive failure. The maximum horizontal displacement occurs at the bottom, accounting for 93.88% of the total displacement.

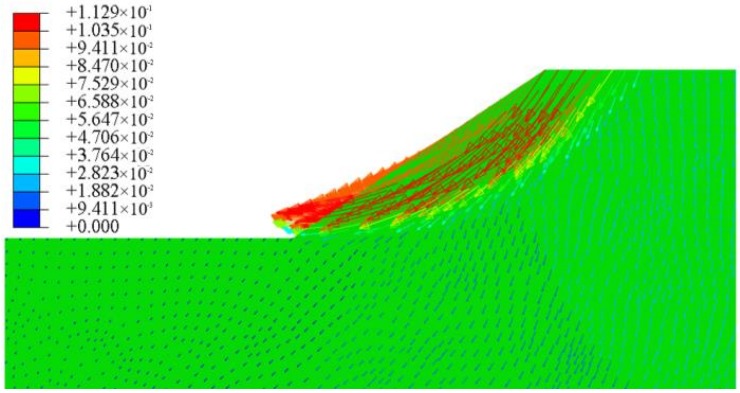

Figure 6. Magnitude displacement vector diagram.

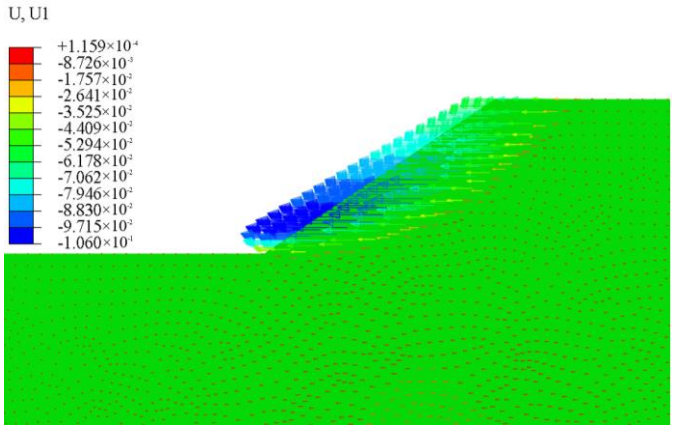

Figure 7. Horizontal displacement vector diagram.

The final safety coefficient is 1.172, which is similar to the conventional calculated safety factor [17], and the related literature [18] stipulates that the stability safety coefficient of slopes at all levels should be greater than 1.35 under the general working condition, and the safety coefficient of the example is lower than that stipulated in the specification, which should be reinforced to make it meet the requirements.

3.3. C30 Concrete Anti-Slip Pile Reinforced Slope Stability Analysis

In most cases, the stability of slopes reinforced with anti-slide piles can be analyzed using 2D models, which offer high computational efficiency and good accuracy [19]. However, to better analyze the location and degree of failure in anti-slide piles and simulate the slope conditions with the piles, this study employed a 3D numerical model. Considering that concrete anti-slide piles may undergo bending failure under lateral soil pressure and that linear elasticity is insufficient to accurately model the entire failure process, a plastic damage model for concrete was used.

Some researchers [20] compared the bending capacity, economic efficiency, and construction duration of three different pile cross-sections and concluded that circular piles are more cost-effective, improve construction efficiency, and adapt better to varied terrain. This study focused on circular piles. A half-pile modeling approach was adopted to reinforce the unstable slope. The slope model remained unchanged, and the pile spacing was set equal to the slope model's thickness (4 m). The boundary conditions of the slope also remained unchanged. The interaction between the piles and the slope soil was modeled as frictional contact, with normal contact defined as "hard" to transmit pressure, and a tangential friction coefficient of 0.3. The simulation consisted of two analysis steps: acquiring the initial geo stress and reducing the soil strength.

Previous studies often used idealized linear elastic models to simulate concrete anti-slide piles, but these models could not capture the plastic failure of concrete under sliding soil pressure, which affected the accuracy of the calculated slope safety factors after reinforcement [21]. It was found that the damage eigenstructure model was used to reflect the softening nature of the piles during the reinforcement process and that the slope safety factor of the piles in the middle of the slope decreased after using the damage eigenstructure [22]. Therefore, this study simulated the response of concrete anti-slide piles using the plastic damage model in ABAQUS. The input parameters for the C30 concrete used in the simulation are shown in Table 2 and Figure 8.

Table 2. Material parameters for concrete anti-slide piles.

Elastic Modulus (kPa)	Poisson's Ratio	Density (kN/m³)	Expansion Angle (°)	Eccentricity	fb_0/fc_0	K	Viscous Parameter
30,000,000	0.20	2.4	30	0.1	1.16	0.667	0.00075

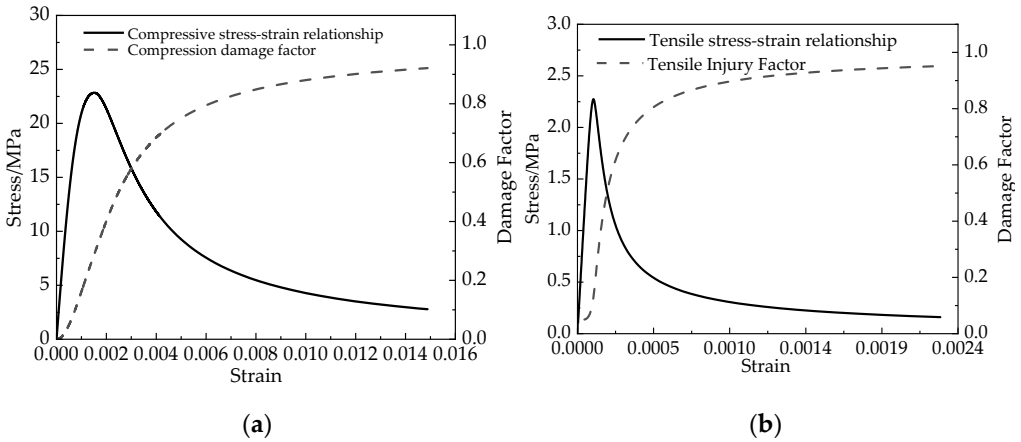

(**a**) (**b**)

Figure 8. Stress–strain and damage factor curves of concrete: (**a**) C30 concrete compressive stress–strain and damage curves; and (**b**) tensile stress–strain and damage curves for C30 concrete.

To investigate the influence of anti-slide pile location and length on the stability of reinforced slopes, nine calculation scenarios were designed. The ratio of the horizontal distance between the pile and the slope crest (a) to the horizontal distance of the slope (b) was used to represent the pile location. To account for location effects, values of a/b were set to 0.1, 0.3, 0.5, 0.7, and 0.9 for simulation. To examine the influence of pile length, the pile top's vertical position relative to the slope was kept constant while the pile length was set to 15 m, 18 m, 21 m, 24 m, and 27 m. For the control groups, the pile length was set to 24 m, and a/b to 0.5.

Figures 9 and 10 show that, as the pile location changed, the maximum stabilizing effect on the slope occurred at a/b = 0.5, with a safety factor of FV1 = 1.45854. The arching effect between piles was strongest at this point, representing a 24.45% improvement over the unreinforced slope's safety factor of 1.172 and meeting the required safety factor of 1.35. The tensile damage analysis revealed that, at a = 0.5 and a = 0.7, the peak tensile damage exceeded 0.8, indicating significant tensile failure. When varying the pile length, the best arching effect occurred with a pile length of 24 m, yielding a slope safety factor of FV1 = 1.47243 and a 25.63% improvement over the unreinforced slope. Among the five lengths tested, only the 15 m pile avoided significant tensile damage, while the remaining four experienced damage, with the largest damage occurring at 24 m.

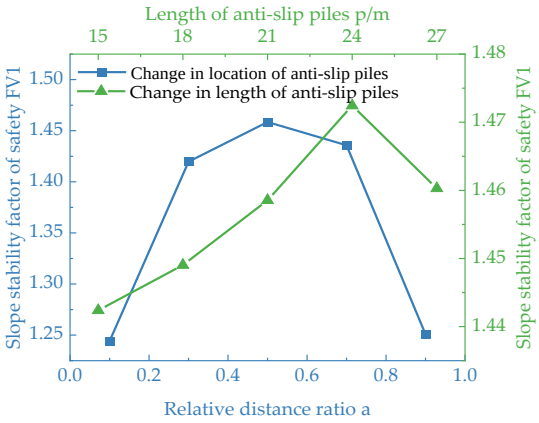

Figure 9. Coefficient of safety FV1 for slope soil stability under the action of C30 concrete anti-slip pile.

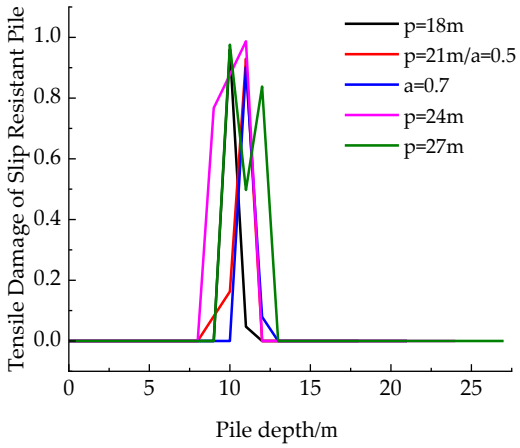

Figure 10. Damage distribution of tensile damage of C30 concrete skid pile.

3.3.1. Analysis of Pile Position Influence

As illustrated in Figure 11a,b, the bending moments and shear forces experienced by the concrete anti-sliding piles vary with their positions. When a = 0.5, the anti-sliding pile experiences maximum bending moment and shear force, with the maximum bending moment reaching 1128 kN/m and the peak shear force being 299.9 kN. This result indicates that, when the anti-sliding pile is positioned in the middle of the slope, it bears the greatest shear and bending moments from the sliding soil mass, resulting in a pronounced arching effect, which enhances the stability of the slope. Conversely, at a = 0.1, the anti-sliding pile exhibits a negative bending moment, indicating the least effective arching effect and the poorest stability. For positions a = 0.3 and a = 0.7, the bending moments and shear forces are only slightly lower than those at a = 0.5. Thus, anti-sliding piles should be positioned centrally to maximize slope stability.

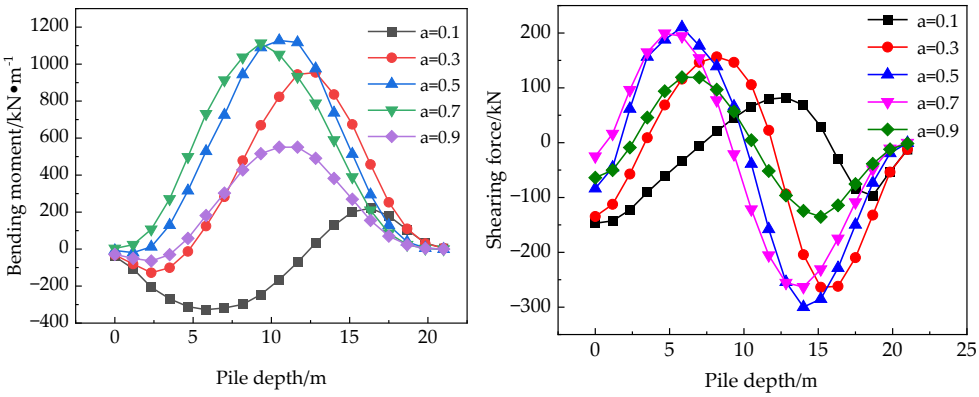

Figure 11. (**a**) Bending moment distribution of anti-sliding piles at different positions; (**b**) shear force distribution of anti-sliding piles at different positions.

From Figure 12a,b, it can be observed that, when the anti-sliding pile is subjected to the action of the sliding soil mass, both the soil stress F1 in front of the pile and the soil pressure F2 behind the pile initially rise before exhibiting a slight decline until a depth of 20 m. This behavior may be related to the detachment that occurs following the deformation of the concrete elements. However, when the pile depth exceeds 20 m, both F1 and F2 experience a sudden increase. The peak soil pressure F1 in front of the pile decreases with an increasing relative distance ratio a; thus, that is to say, the closer the anti-slip pile is to the lower position of the slope, the greater the landslide soil force it is subjected to. The soil pressure F2 behind the pile is minimized at a = 0.5 and a = 0.7, which are also the positions where the arching effect of the anti-sliding pile is most significant.

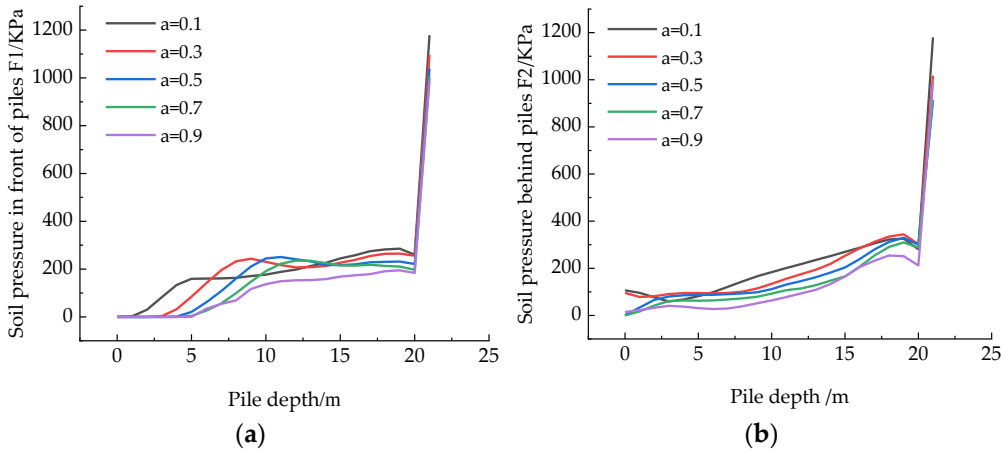

Figure 12. (**a**) Soil pressure distribution in front of anti-sliding piles at different positions; (**b**) soil pressure distribution behind anti-sliding piles at different positions.

Slip-resistant piles play a role in slope stabilization by bridging the displacements of sliding and stabilizing soils and preventing the emergence of a soil-slip interface. The displacement of the anti-slip pile in the sliding soil body is large, and the displacement in the stable soil body is small, so the anti-slip pile bending moment occurs in the position where the sliding interface should have appeared, and the peak position of the bending moment, the magnitude of the shear force, the size of the pile front soil pressure, and the position of the sudden change in the soil pressure after the pile can be regarded as the position of the sliding interface and as the key design position of the pile cross-section and the pile body material.

The plastic damage analysis of anti-sliding piles at different positions, as shown in Figure 13, indicates that, when a = 0.5 and a = 0.7, the tensile damage significantly exceeds the failure threshold of 0.8, resulting in pronounced bending and tensile failure. This finding correlates with the substantial arching effect observed, which significantly enhances the slope stability safety factor FV1. In other positions, no noticeable plastic damage occurs in the anti-sliding piles. During the process of stabilizing the slope, the concrete anti-sliding piles did not exhibit compressive damage, with all compressive damage values remaining below 0.1, indicating that they were in a safe compressive state.

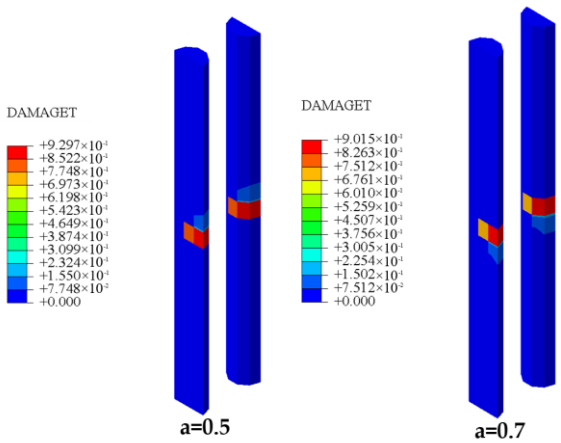

Figure 13. Distribution cloud map of tensile damage in anti-sliding piles at different positions.

3.3.2. Analysis of the Influence of Pile Length

The distribution of bending moments and shear forces of anti-sliding piles at different lengths concerning pile depth is illustrated in Figure 14a,b. From the content of this figure, it can be observed that, when the length of the anti-sliding pile reaches 24 m, the maximum bending moment and shear force are achieved, with a maximum bending moment of

1207 kN/m and a maximum shear force of 311 kN. This finding indicates that, when p = 24 m, the anti-sliding pile exerts the greatest earth arch effect to stabilize the sliding slope. The distribution of bending moments and shear forces under the action of sliding soil remains nearly consistent across different pile lengths.

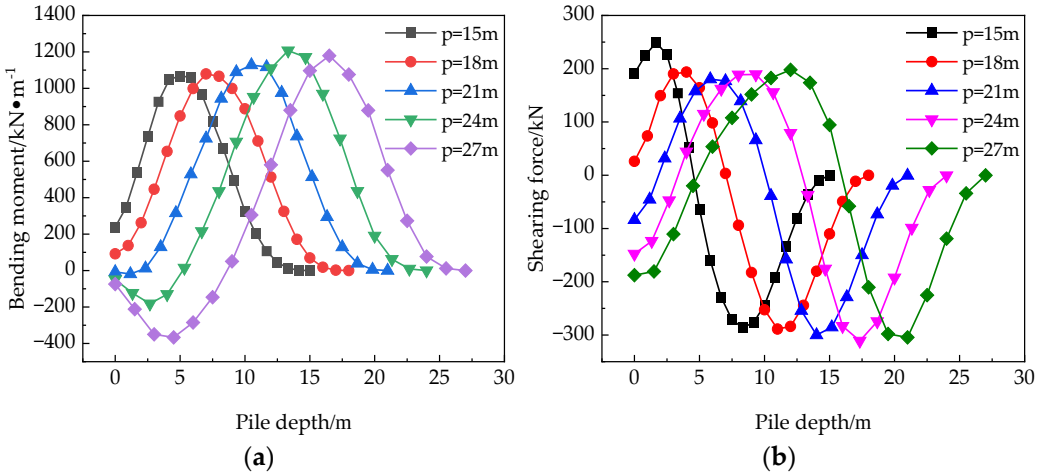

Figure 14. (**a**) Distribution of bending moments in anti-sliding piles of different lengths; (**b**) distribution of shear forces in anti-sliding piles of different lengths.

As shown in Figure 15a,b, compared to the soil pressure distribution of the pile when the position of the anti-sliding pile is altered, the distribution of soil pressures when changing the length of the anti-sliding pile exhibits a more pronounced correlation with pile length, primarily reflected in the back soil pressure. The peak value of the back soil pressure increases with the length of the anti-sliding pile. When p = 15 m, there is no significant increase in back soil pressure; the pile is too short to reach the plastic zone of the soil slope, rendering it unable to stabilize the slope effectively.

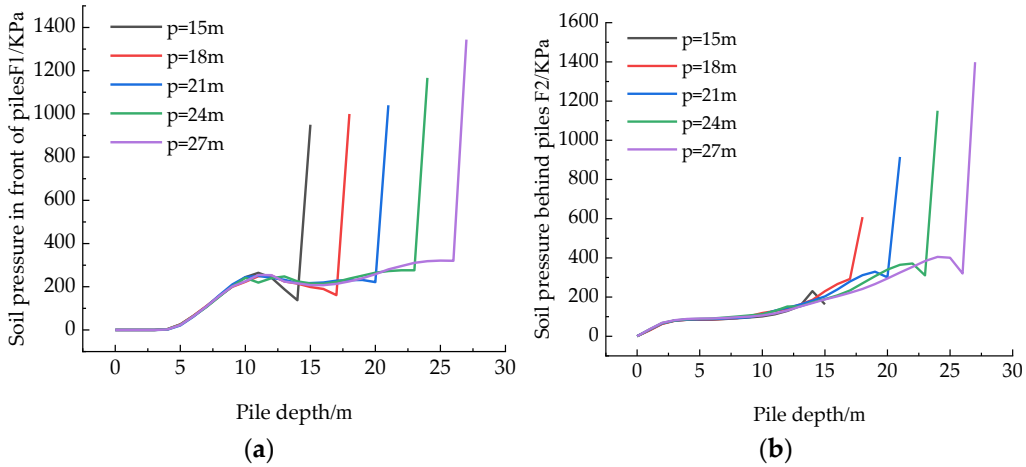

Figure 15. (**a**) Distribution of front soil pressure in anti-sliding piles of different lengths; (**b**) distribution of back soil pressure in anti-sliding piles of different lengths.

From Figure 16, it can be seen that, in the simulation calculations for five different lengths of anti-sliding piles, except for the case where p = 15 m, the tensile plastic damage in anti-sliding piles exceeds the failure threshold of 0.8, indicating tensile failure. The damage areas are mainly concentrated within 10 m from the top of the anti-sliding pile, while no compressive damage occurs in the piles.

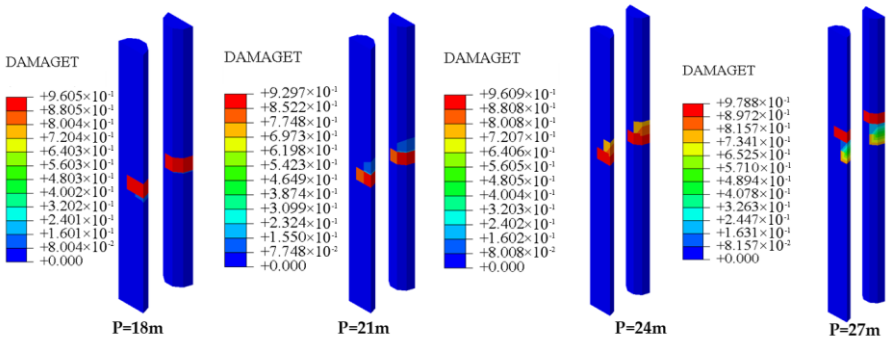

Figure 16. Distribution cloud map of tensile damage in anti-sliding piles of different lengths.

Based on the above calculations, it can be concluded that, when anti-sliding piles are constructed using conventional concrete materials to stabilize slopes, they are prone to bending failure in certain conditions due to insufficient bending strength and toughness, which may lead to failure in resisting the forces exerted by the slope soil. Currently, high-toughness cement-based materials exhibit superior bending toughness and strength, and their engineering applications have proven effective. However, there is limited research on applying these materials to the stabilization of slopes using anti-sliding piles. Most studies focus on enhancing the slope stability safety factor by adjusting pile spacing, length, and position, with few examining whether the anti-sliding piles themselves incur damage, especially bending failure. Therefore, this study aims to improve the bending toughness of the materials used in anti-sliding piles to enhance their stability against landslides.

3.4. Stability Analysis of Slope Reinforcement Using High-Toughness Concrete Anti-Sliding Piles

The physico-mechanical parameters of the materials measured in this study through tests such as axial compression are shown in Table 3, which provides a theoretical basis for modeling the performance enhancement effect of the tunnel lining. These parameters include the following: the selection of good tensile and bending properties of the ratio for the lining of high-toughness cementitious composites of the principal parameters of this study, the obtained test stress–strain relationship is fitted, the calculation of the lining of high-toughness cementitious composites of the principal parameters of the calculation of the calibration of the lining of high-toughness cementitious composites of the principal parameters of Figure 17, and its numerical simulation calculations for comparison of the effect of the application.

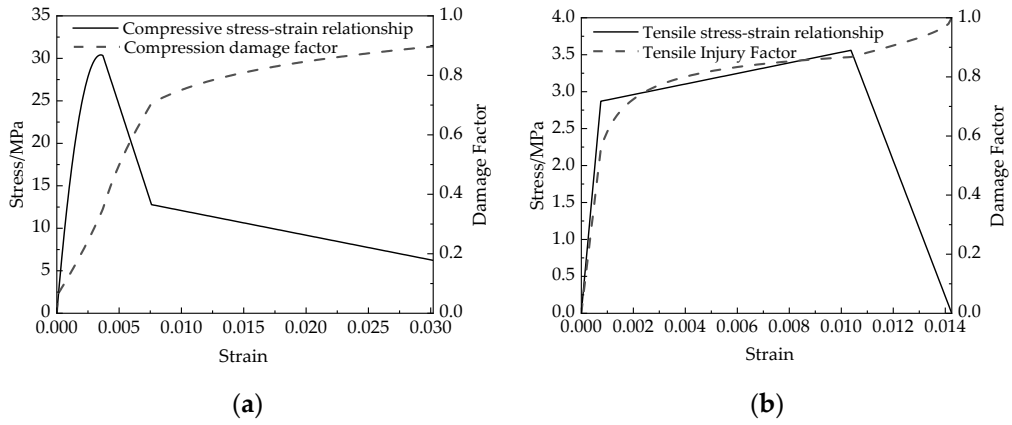

Figure 17. Stress–strain and damage curves of high-toughness cement-based composite materials: (**a**) compression stress–strain and damage curve; and (**b**) tension stress–strain and damage curve.

Table 3. Material parameters of the slope soil.

Material	Elastic Modulus (MPa)	Poisson's Ratio	Density (kg/m³)
High Toughness Cement-Based Composite	19,461	0.2	2102

The simulation calculation scheme for the high-toughness anti-sliding piles was the same as that for conventional concrete anti-sliding piles. As shown in Figure 18, with changes in the position and length of the anti-sliding piles, the variation pattern of the slope stability safety factor FV1 is consistent with that of conventional concrete anti-sliding piles. Considering the position of the anti-sliding piles, at a = 0.1 and a = 0.9, there is no significant improvement in FV1 for high-toughness anti-sliding piles compared to conventional concrete anti-sliding piles. In these two positions, improving the bending toughness of the anti-sliding pile materials does not enhance the slope's safety performance. At a = 0.5, the slope stability safety factor FV1 reaches its maximum value of 1.54822, which is a 32.10% increase over the safety factor of 1.172 for the unreinforced slope, demonstrating a more pronounced improvement compared to conventional concrete anti-sliding piles. Furthermore, when considering the length of the anti-sliding piles, it was observed that the application of high-toughness anti-sliding piles significantly increases FV1 for different lengths, with the maximum safety factor reaching 1.55804 at p = 24 m.

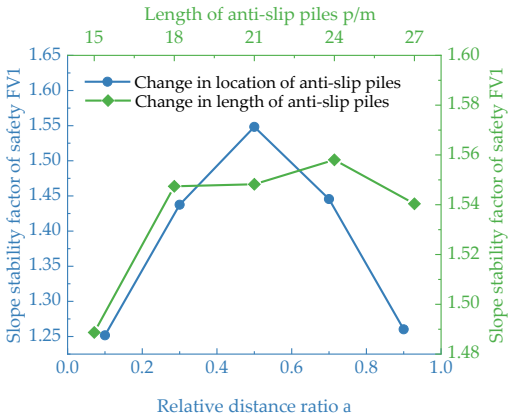

Figure 18. Coefficient of safety FV1 of slope soil stability under the action of high-toughness concrete anti-slip pile.

An analysis of the plastic damage in the high-toughness anti-sliding piles shown in Figure 19 indicates that there is no tensile damage at a = 0.7, while tensile failure only occurs in four working conditions at the middle position of the slope.

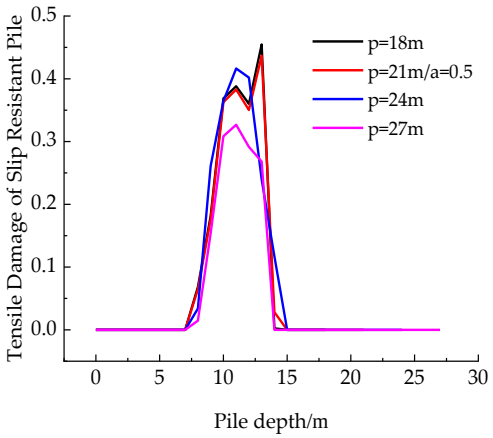

Figure 19. Tensile damage distribution in ECC anti-sliding piles.

3.4.1. Analysis of Pile Position Influence

As illustrated in Figure 20a,b, the bending moment and shear force of high-toughness anti-sliding piles reach their maximum at a = 0.5, with the maximum bending moment of 1752 kN/m and the maximum shear force at 391.1 kN. This finding represents an increase of 35.61% and 30.41%, respectively, compared to conventional concrete piles, attributed to the superior tensile and flexural toughness of the high-toughness cement-based composite materials, enabling them to withstand greater bending moments and shear forces.

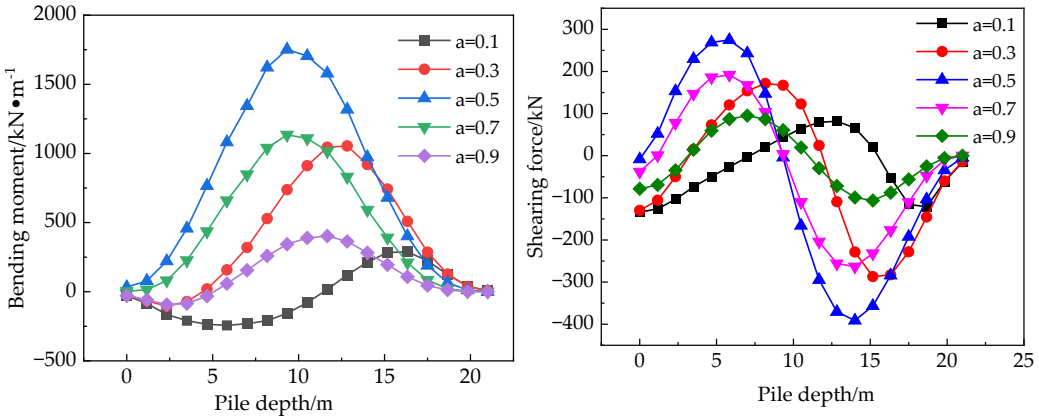

Figure 20. (**a**) Bending moment distribution of ECC anti-sliding piles at different positions; (**b**) shear force distribution of ECC anti-sliding piles at different positions.

From Figure 21a,b, it can be observed that, after changing the position of the anti-sliding piles, the soil pressures acting on the pile front (*F*1) and pile back (*F*2) for high-toughness anti-sliding piles show no significant difference in peak values compared to those of conventional concrete piles, and their variation patterns remain consistent. Specifically, the pile front soil pressure *F*1 decreases as the relative distance ratio a increases.

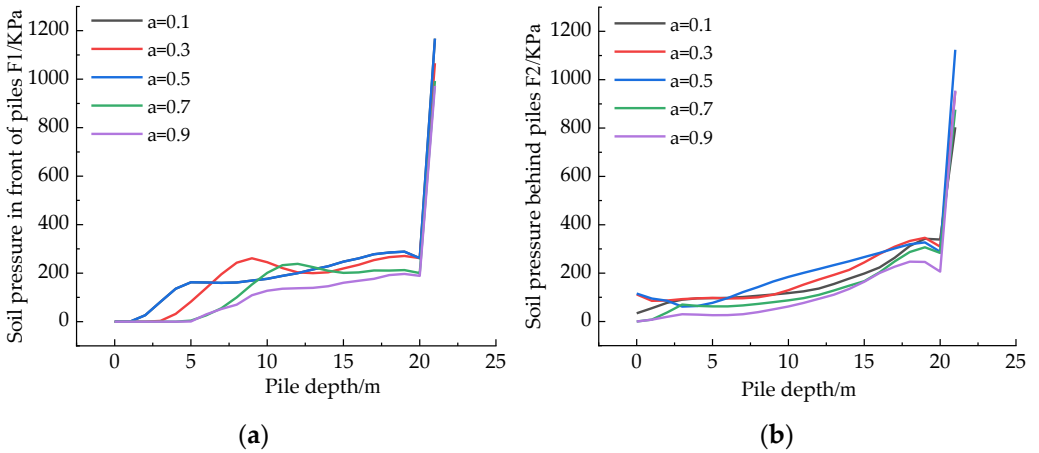

Figure 21. (**a**) Distribution of pile front soil pressure F1 for ECC anti-sliding piles at different positions; (**b**) distribution of pile back soil pressure F2 for ECC anti-sliding piles at different positions.

3.4.2. Analysis of the Effect of Pile Length

Figure 22a,b illustrates the distribution of the bending moment and shear force under different lengths of ECC anti-sliding piles. At a pile length of p = 24 m, the high-toughness anti-sliding piles exhibit the highest bending moment of 1793 kN/m and a maximum shear force of 392.8 kN, representing increases of 48.56% and 26.3%, respectively, compared to conventional concrete piles. This finding indicates that high-toughness anti-sliding piles

can withstand larger bending moments and shear forces, facilitating the development of the soil arching effect.

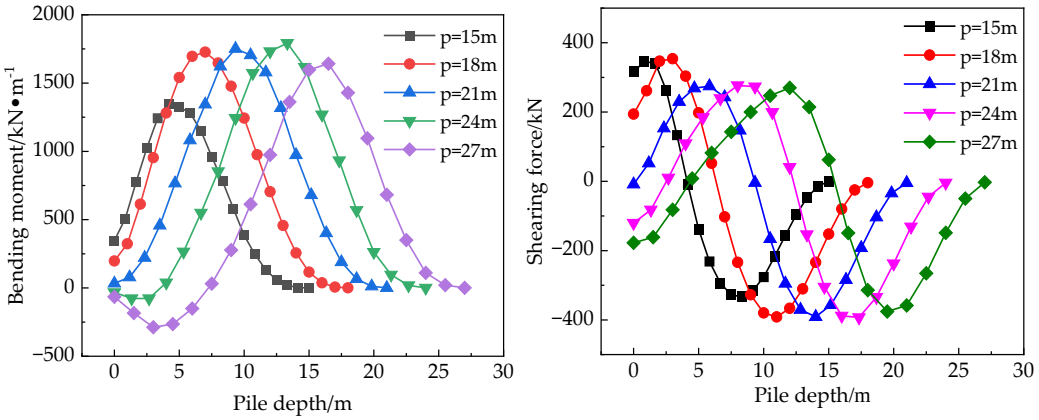

Figure 22. (**a**) Bending moment distribution of ECC anti-sliding piles of different lengths; (**b**) shear force distribution of ECC anti-sliding piles of different lengths.

As shown in Figure 23a,b, after changing the length of the anti-sliding piles, the pile front soil pressure *F*1 experiences a sharp peak increase at the pile base. At lengths of p = 15 m and p = 18 m, the pile back soil pressure *F*2 does not show a sharp increase, possibly due to soil bending causing a gap, which prevents the pile from effectively stabilizing the soil.

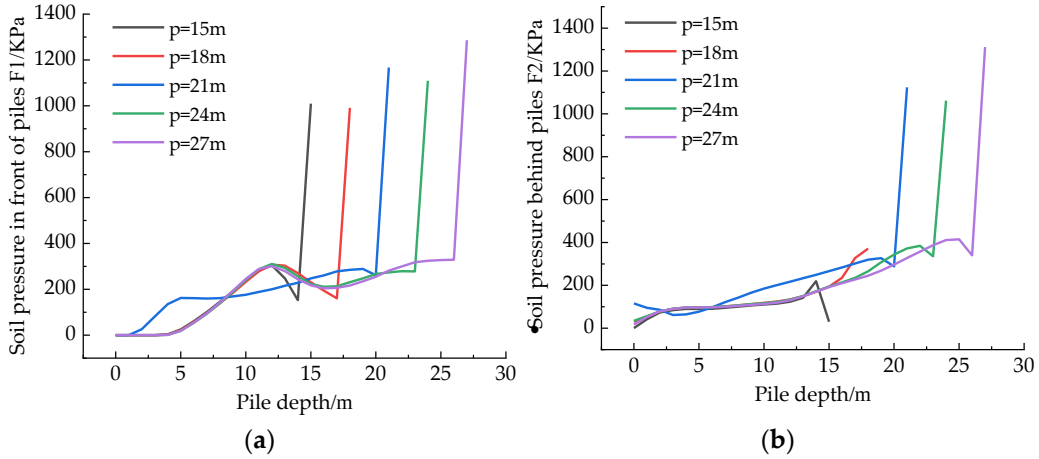

Figure 23. (**a**) Distribution of pile front soil pressure F1 for ECC anti-sliding piles of different lengths; (**b**) distribution of pile back soil pressure F2 for ECC anti-sliding piles of different lengths.

From Figure 24, it can be concluded that the high-toughness anti-sliding piles exhibit notable tensile failure when changing the length of the piles. Tensile plastic damage occurs only at the contact point of the sliding surface of the soil, with maximum tensile damage recorded at p = 24 m at a value of 0.558, which is below the failure threshold of 0.8. The use of high-toughness cement-based composite materials significantly enhances the tensile toughness of the anti-sliding piles, thereby preventing bending failure.

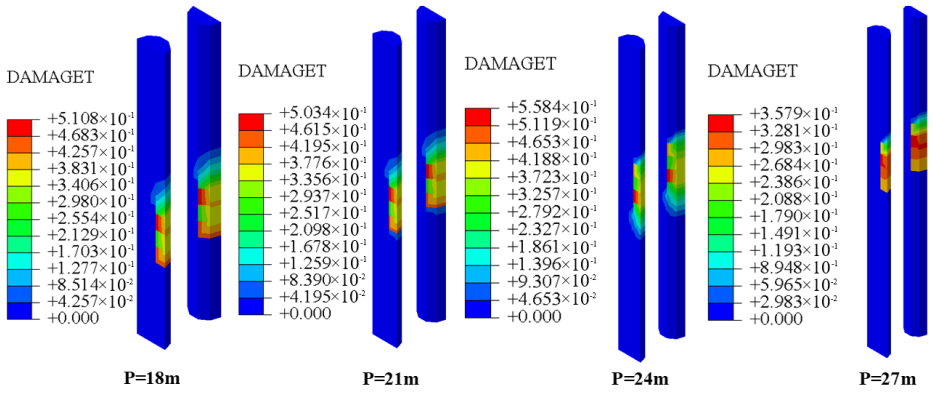

Figure 24. Distribution of tensile damage in ECC anti-sliding piles of different lengths.

3.5. Expansion of Design Methods to Cope with Different Soils

In this paper, only the applicability research and design optimization of high tenacity skid resistant piles in the soil parameters and slope dimensions under the actual condition of the dependent project are carried out, and the specific parameters of the optimized design and the stability enhancement effect are somewhat different in the face of different soil and slope dimensions. However, the superiority of anti-slip piles made of high-toughness concrete material and the method of obtaining the specific parameters of optimization design is the same, so we can use Isight software (version number: Isight 2023x) to carry out the DOE pre-optimization design of different material parameters and different soil sizes, take the minimization of slope displacement and the maximum tensile stress of anti-slip piles as the design objectives, derive the pile length, the relative distance ratio, the material parameters of the soil, and the slope gradient with the design objectives. The relationship between pile length, relative distance ratio, soil material parameters, slope gradient, and the design objective is determined, and a suitable approximation model type is selected for approximation modeling. Finally, a reasonable approximation formula is obtained to simplify its application; in the case of less than ideal simulation results, we can also use Isight to encapsulate the whole optimization design process and simplify the optimization design process in different application scenarios through parameterized modeling and DOE design optimization.

4. Conclusions

This study, based on the Urban-Rural Integration Water Supply Project in Lingao County, proposes the use of anti-sliding piles to enhance the stability of excavation slopes. By simulating and analyzing typical slope cases, this research investigates the stability safety factor FV1 of the slope soil under different positions and lengths of anti-sliding piles and emphasizes the improvement of the bending toughness of the anti-sliding pile materials to enhance their stability against landslides. The following conclusions are drawn:

1. For nonlinear analyses that require assessing the type of landslide and the position of the sliding surface, a comprehensive approach incorporating numerical simulation convergence, the continuity of the slope's plastic zone, and a rapid increase in displacement at a specific point on the slope offers a more accurate assessment of slope instability;
2. The position and length of anti-sliding piles significantly affect slope stability. When the relative distance ratio a = 0.5, the stabilizing effect of the anti-sliding piles on the slope soil is maximized, achieving a stability safety factor FV1 of 1.45854, representing a 24.45% improvement over the unreinforced slope. For a pile length of p = 24 m, the soil arching effect is optimal, yielding a stability safety factor FV1 of 1.47243, which is a 25.63% increase compared to the unreinforced slope;
3. High-toughness material anti-sliding piles exhibit superior mechanical properties compared to conventional concrete anti-sliding piles. At a = 0.5, the application of

high-toughness material anti-sliding piles achieves a stability safety factor FV1 of 1.54822, reflecting a 32.10% improvement over the unreinforced slope and a 7.55% improvement over conventional concrete anti-sliding piles. The maximum safety factor is 1.55804 when the pile length is p = 24 m;

4. Optimization in design is crucial for leveraging the advantages of high-toughness materials. By strategically designing pile positions and lengths, the reinforcement effectiveness of high-toughness material anti-sliding piles can be maximized.

Author Contributions: Conceptualization, C.X.; Formal analysis, C.X.; Data curation, C.X.; Methodology, C.X. and Y.Y.; Resources, C.X.; Investigation, Y.Y., D.L. and W.L.; Writing—original draft, Y.Y.; Supervision, C.Z.; Validation, C.Z., H.L., L.G. and C.W.; Writing—review &editing, C.Z.; Funding acquisition, D.L. and L.G.; Project administration, Y.Y. and C.W. All authors have read and agreed to the published version of the manuscript.

Funding: This research was funded by [R&D Project of Originwater Construction Group Co.] grant number [ZJLJ-HCZQ-4B-01-ZJBSY-2024-004] and funded by Dayu Liu and Liying Guo.

Data Availability Statement: The original contributions presented in the study are included in the article, further inquiries can be directed to the corresponding author.

Conflicts of Interest: Authors Changzhu Xing, Yanwei Yang, Dayu Liu, Haigang Li, Liying Guo, Weitao Lin and Chengda Wang were employed by the company Originwater Construction Group Co., Ltd. The remaining author declares that the research was conducted in the absence of any commercial or financial relationships that could be construed as a potential conflict of interest.

References

1. Zhu, D.; Jiang, G.-L.; Chen, H.-Y.; Zhao, X.-H.; Huang, D.-G.; Liu, Y.-F. Shaking Table Experimental Study on the Dynamic Response Characteristics of Single and Double-Row Pile-Supported Road Graben Slopes. *Rock Soil Mech.* **2024**, *45*, 1763–1777. [CrossRef]
2. Zheng, X.; Cheng, C.; Yuan, W. Bionic Anti-Slipping Crimping Structure for Industrial Hose Assembly Inspired by Ruminant Molars. *Appl. Bionics Biomech.* **2022**, *2022*, 5632586. [CrossRef] [PubMed]
3. Zhang, S.; Yang, Z.; Liu, Q.; Fan, W.; Zhang, G.; Zhang, X. Analysis of Influence Factors of Anti-Slide Pile with Prestressed Anchor Cable Based on Bearing and Deformation Characteristics of Pile Body. *Sustainability* **2023**, *15*, 10549. [CrossRef]
4. Zhang, N.; Luo, B.; Huang, L.; Luo, M. Research on the Anti-Slip Performance of Arc Groove Cable Clamps. *J. Constr. Steel Res.* **2024**, *220*, 108858. [CrossRef]
5. Zhang, J.; Ma, J.; Ma, K.; Tan, Y.; Yan, Z.; Feng, J. Treatment Measures for the Creep-Slip Phase of Landslides Induced by Twin Tunnels. *Proc. Inst. Civ. Eng. Geotech. Eng.* **2023**, *176*, 525–537. [CrossRef]
6. Zhang, C.; Shi, C.; Dong, J.; Zhang, L. Numerical Simulation of Three-Dimensional Soil Arch Effect between h-Type Pile-Based Discrete Element Method. *Nat. Hazards* **2024**, *120*, 8283–8301. [CrossRef]
7. Yu, R.; Huang, Z.; Yang, Z. Slope Reinforcement Design Based on Geostudio and Flac3d. *Min. Sci.* **2022**, *29*, 144–163. [CrossRef]
8. Yao, Y.; Hong, B.; Liu, X.; Wang, G.; Shao, Z.; Sun, D. Field and Numerical Study of the Bearing Capacity of Pre-Stressed High-Strength Concrete (PHC)-Pipe-Pile-Reinforced Soft Soil Foundations with Tie Beams. *Appl. Sci.* **2023**, *13*, 11786. [CrossRef]
9. Jin, Y.; Zhao, H.; Zheng, C.; Liu, J.; Ding, C. Effect of Steel Support Cross-Section and Preloaded Axial Force on the Stability of Deep Foundation Pits. *Buildings* **2024**, *14*, 2532. [CrossRef]
10. Yang, Y.; Ling, L.; Wang, J.; Zhai, W. A Numerical Study on Tread Wear and Fatigue Damage of Railway Wheels Subjected to Anti-Slip Control. *Friction* **2023**, *11*, 1470–1492. [CrossRef]
11. Yang, Y. Influence of Basalt Fiber-Reinforced Cement-Based Composite on Slope Stability. *J. Compos. Adv. Mater./Rev. Compos. Matériaux Avancés* **2021**, *31*, 93–100. [CrossRef]
12. Nassiraei, H. Probabilistic Analysis of Strength in Retrofitted X-Joints under Tensile Loading and Fire Conditions. *Buildings* **2024**, *14*, 2105. [CrossRef]
13. Xu, J.; Jia, Y.; Liu, J.; Asheghabadi, M.S.; Wang, Y. Study on the Stability of Accumulation Using a Slope Shaking Table Test during Earthquake Action. *Buildings* **2024**, *14*, 2. [CrossRef]
14. Xin, C.; Yang, F.; Feng, W.; Li, W.; Liao, J. Shattering Failure Mechanism of Step-like Bedding Rock Slope under Multi-Stage Earthquake Excitations. *Rock Soil Mech.* **2023**, *44*, 3481–3494. [CrossRef]
15. Wang, Z.; Han, Q.; Lu, Y.; Hu, Y. Anti-Slip Performance of Cast Steel Cable Clamps for Prestressed Cables. *Structures* **2022**, *46*, 353–368. [CrossRef]
16. Wang, Y.; Yuan, L.; Chen, H.; Du, P.; Lian, X. An Anti-Slip Control Strategy with Modifying Target and Torque Reallocation for Heavy in-Wheel Motor Vehicle. *Proc. Inst. Mech. Eng. Part J. Automob. Eng.* **2022**, *236*, 2625–2644. [CrossRef]

17. Wang, S.; Wang, J.; Chen, Y.; Zhang, Y. A Method for Calculating the Lateral Earth Pressure on Rigid Anti-Slip Piles with EPS Inclusions. *Proc. Inst. Civ. Eng. Geotech. Eng.* **2024**. [CrossRef]
18. Tian, W.; Zhou, K.; Chen, Z.; Shen, Z.; Wang, Z.; Jiang, L.; Cong, Q. Design of Bionic Foot Inspired by the Anti-Slip Cushioning Mechanism of Yak Feet. *Biomimetics* **2024**, *9*, 260. [CrossRef]
19. Pei, Z.; Zhang, Y.; Nian, T.; Xiao, S.; Liu, H. Cross-Scale Analysis on the Working Performance of Micropile Group and Talus Slope System. *Sustainability* **2023**, *15*, 8154. [CrossRef]
20. Li, Y.; Xie, X.; Jin, B.; Chen, L.; Liang, X.; Yin, K. Comprehensive Risk Management of Reservoir Landslide-Tsunami Hazard Chains: A Case Study of the Liangshuijing Landslide in the Three Gorges Reservoir Area. *Landslides* **2024**. [CrossRef]
21. Li, X.; Ran, Y.; Wang, K.; Shi, Z. Study of Load Calculation Models for Anti-Sliding Short Piles Using Finite Difference Method. *Appl. Sci.* **2023**, *13*, 12399. [CrossRef]
22. Kim, Y.; Kwon, S. Balancing-Prioritized Anti-Slip Control of a Two-Wheeled Inverted Pendulum Robot Vehicle on Low-Frictional Surfaces with an Acceleration Slip Indicator. *Machines* **2023**, *11*, 553. [CrossRef]